Fatigue Analysis of Temporary Offshore Structures using Monte Carlo Simulations

submitted on 31 August 2022

by

JENS Katharina

ULiège Student ID No.: S203829

First Reviewer:

Pablo Gabriel Morato Dominguez, PhD

University of Liège (ANAST)

Allée de la Découverte 9

4000 Liège

Belgium

Second Reviewer:

Antonio Medina Mánuel, MSc

Polytechnic University of Madrid (CEHINAV)

Avd. de la Memoria 4

28040 Madrid

Spain

[This page is intentionally left blank.]

CONTENT

LIST OF FIGURES

LIST OF TABLES

DECLARATION OF AUTHORSHIP

I declare that this thesis and the work presented in it are my own and have been generated by me as the result of my own original research.

Where I have consulted the published work of others, this is always clearly attributed. Where I have quoted from the work of others, the source is always given. With the exception of such quotations, this thesis is entirely my own work. I have acknowledged all main sources of help. Where the thesis is based on work done by myself jointly with others, I have made clear exactly what was done by others and what I have contributed myself.

This thesis contains no material that has been submitted previously, in whole or in part, for the award of any other academic degree or diploma.

I cede copyright of the thesis in favour of the University of Madrid.

Date: 31.08.2022 Signature:

ABSTRACT

The *Orion*, an offshore heavy lift DP3 installation vessel owned by DEME Group, is deployed worldwide to install monopiles of up to 2,500 tons with its 5,000-ton crane. A seafastening structure holding the monopiles on board of the vessel is exposed to cyclic loading due to waves encountered at sea. The fatigue life of this monopile seafastening, therefore, needs to be analyzed to ensure its integrity during installation and transport operations. For this, the applicability of different fatigue estimation methods is investigated throughout the thesis.

Firstly, simplified fatigue analysis methods are tested to obtain an order of magnitude of the expected fatigue damage and to determine its criticality. The lambda factor method is adapted to offshore structures providing an approach to represent a variable load history by estimating equivalent stress cycles at a constant stress range. In another simplified method, the fatigue damage is approximated using a weighted sum approach. By calculating the fatigue damage for one hour spent in specified nautical areas, the total damage of different operational profiles can easily be assessed. This approach is further developed by applying the Monte Carlo technique to determine the damage expected for one hour of operation.

Secondly, Monte Carlo simulations are implemented in Python to study the fatigue life of the seafastening in detail. In the simulation, the considered sea states are defined based on scatter diagrams and the vessel's motion response is determined for every hour of operation. The stress ranges resulting from the accelerations of the monopile, as well as the number of stress cycles that the seafastening structure on the vessel experiences are calculated. Based on the stress occurrences, the partial fatigue damage of every hour and, ultimately, the total fatigue damage are estimated. By varying the input parameters of the analysis and evaluating the effect on the fatigue damage, recommendations on the optimal operational profile with respect to the fatigue life of the seafastening are made.

In this public version, the results such as the predicted fatigue life and damage values are not included.

[This page is intentionally left blank.]

1 INTRODUCTION

The current advancements in the offshore wind industry lead to the installation of turbines with ever-increasing capacity. Therefore, there is a demand of installation vessels able to handle the growing turbines and their supporting structures. DEME is meeting this demand with its new offshore heavy lift vessel *Orion* which is equipped with the necessary tools to transport and install monopiles, which are the most common foundation type of offshore wind turbines. During the transportation phase, the monopiles need to be secured by a seafastening. Traditionally, seafastening structures are designed to be a disposable tool and used for one project only. DEME has made advances in the past to design reusable seafastening, continuing this change with the monopile seafastening installed on the *Orion* that is planned to be used for an operational time of at least ten years. As every project has its own specific foundations with changing dimensions, an innovative seafastening structure was developed that can be adjusted to the diameter of the pile used in the current project. This adaptable design provides flexibility in the deployment of the *Orion* and the seafastening's capacity of holding a 2500-ton monopile is a forward-looking investment considering the trend of increasing monopile dimensions.

The seafastening onboard of a vessel is subjected to cyclic loading due to the encountered waves. Even though offshore operations such as the installation of turbine foundations are carried out in restricted environmental conditions, these loads could lead to a fatigue failure. Consequently, the fatigue life of the seafastening structure needs to be studied to ensure its integrity during the entire planned operational period. This thesis analyzes if the planned operations are feasible with regards to the caused fatigue damage and the remaining fatigue life is assessed for the planning of future projects.

The study mainly focusses on the estimation of loading cycles and their corresponding stress ranges based on a given operational profile. For this, different simplified fatigue analysis methods are tested to determine the criticality of the expected fatigue damage. Monte Carlo simulations are applied to simulate the operational life of the seafastening and quantify the fatigue. In a sensitivity study, the influence of multiple environmental parameters, such as the wave encountering angle, on the fatigue damage are investigated.

1.1 Study Case

The temporary offshore structure studied in this thesis is the monopile (MP) seafastening of DEME Offshore's floating heavy lift vessel *Orion*. In the following, both the vessel and the seafastening structure are introduced. Furthermore, the planned operations are presented.

1.1.1 Orion

The *Orion* is an offshore heavy lift installation vessel with a DP3 dynamic positioning system that was delivered in 2019. The vessel has a length of 216.5 m, a breadth of 49 m and a depth of 16.8 m. Its main crane has a lifting capacity of 5,000 tons. The auxiliary capacity is 1,500 tons and additionally two knuckle boom cranes with 100 tons capacity are installed on the ship. With a maximum pay load of 30,000 tons and a free deck area of 8,000 m^2, the ship can be deployed for many different activities including the transport of monopiles (MPs) to the project site as shown in Figure 1. A motion compensated pile gripper supports the upending of monopiles and stabilizes the foundations during their installation (see Figure 2). Noise mitigation systems are integrated in the gripper tool to reduce the noise while the monopiles are hammered into the seabed. The dynamic positioning system in combination with a total of eight thrusters enable the vessel to accurately hold position during operations without mooring. Accommodations for 160 crew members are available on the *Orion* (DEME, n.d.).

Figure 1: Heavy Lift Vessel *Orion*

Figure 2: *Orion* during Installation

1.1.2 Planned Route

1.1.3 Seafastening

1.2 Conventions

In this section, the conventions followed in this thesis are presented. The degrees of freedom and the coordinate system used throughout the thesis are presented in Figure 3. The x-axis is positive towards the bow of the vessel, the y-axis points to the portside and the z-axis upwards. The designation of the translational and rotational degrees of freedom with their positive direction indicated by the arrow directions are given.

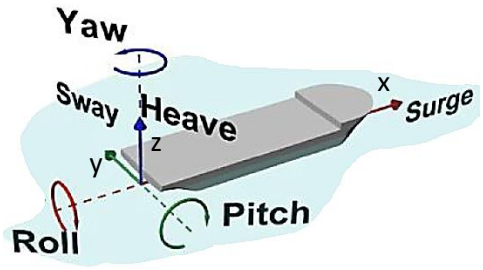

Figure 3: Definition of Degrees of Freedom

The wave encountering angles with respect to the vessel and corresponding descriptions are shown in Figure 4. The directions are defined between 0˚at the stern to 180˚ at the bow. Wave angles on the starboard are positive and on the portside negative. Head seas can be expressed as an angle of wave encounter of 180˚ or -180˚.

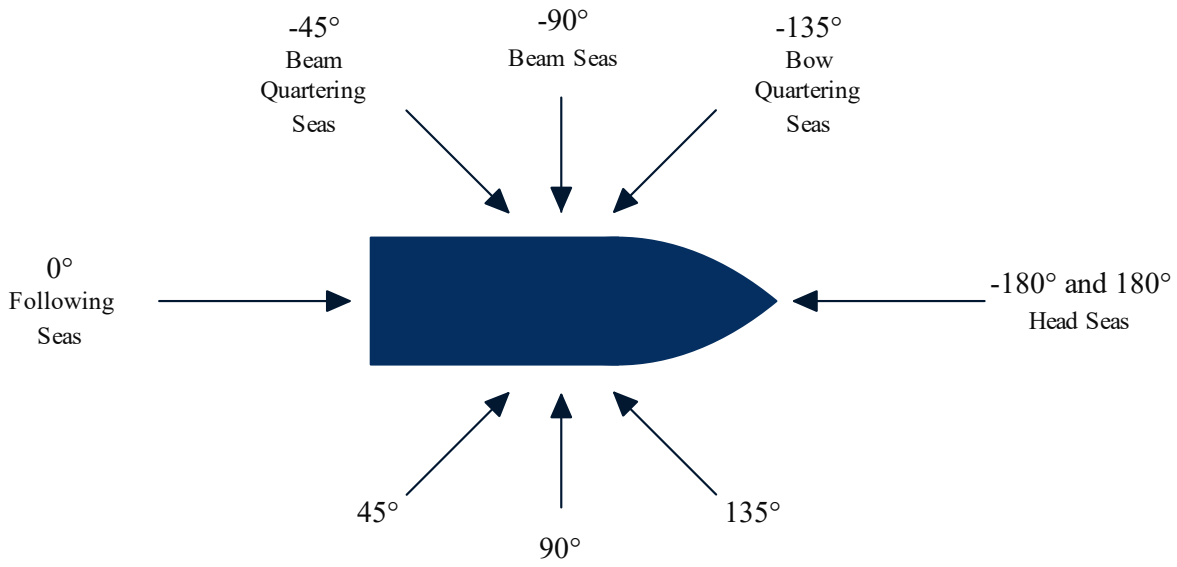

Figure 4: Definition of Wave Encountering Angles

2 HYDRODYNAMICS

This chapter introduces the hydrodynamic theories used in this thesis to analyze the seakeeping parameters of the *Orion* relevant for the fatigue estimation. Based on Newton's second law, the equation of motion for a ship is derived and the response amplitude operator (RAO) is defined. Both can be solved using radiation-diffraction analyses which can be conducted in software such as ANSYS Aqwa. The importance of the correct estimation of roll damping is highlighted and a method to determine roll damping coefficients is presented. Wave energy spectra are introduced and combined with the RAOs to obtain response spectra. The acceleration response spectra with the significant accelerations as well as the stress response spectrum with the significant stresses are defined.

2.1 Equation of Motion

The equation of motion of a rigid body is based on Newton's second law of motion and is given in Equation (1) for a structure at sea:

$$F = ma = m\ddot{s} = F_h + F_e \tag{1}$$

where m is the mass of the body, a and $\ddot{s}$, respectively, are its accelerations, and F_e is the wave excitation force. F_h are hydromechanical forces which are the reaction forces of the water. They consist of the added mass, the damping and the hydrostatic restoring force which depends on the buoyancy of the body and the gravity forces acting on it. With $F_h = -Cs - B\dot{s} - A\ddot{s}$, the equation of motion for a rigid body with six degrees of freedom can be expressed as shown in Equation (2):

$$M\ddot{s} = -Cs - B\dot{s} + F_e - A\ddot{s} \tag{2}$$

where C is the stiffness matrix, B is the damping matrix, A is the added mass matrix and M is the mass matrix, which can be determined from determined from the lightship weight and the weight distribution of the vessel (Journée & Massie, 2001). From this, the wave excitation force F_e is obtained as given in Equation (3):

$$(M + A)\ddot{s} + B\dot{s} + Cs = F_e \tag{3}$$

The response motion *s*, velocity $\dot{s}$ and acceleration $\ddot{s}$ are defined as shown in Equation (4) to (6) depending on the response amplitude $\hat{s}$:

$$s = \hat{s}e^{i\omega t} \tag{4}$$

$$\dot{s} = i\omega\hat{s}e^{i\omega t} \tag{5}$$

$$\ddot{s} = -\omega^2\hat{s}e^{i\omega t} \tag{6}$$

where ω is the angular wave frequency and *t* is the time. Finally, the excitation force can be expressed as a function of the amplitude $\hat{s}$ as shown in Equation (7) (Newman, 1977).

$$[-\omega^2(M + A) + i\omega B + C]\hat{s} = F_e \tag{7}$$

The wave excitation force is composed of the diffraction force and the Froude-Krylov force. The diffraction force is a force on a structure due to disturbance of the wave caused by the body. The Froude-Krylov force is caused by the pressure field of undisturbed waves. Both are non-viscous forces (Faltinsen, 1998).

2.2 Response Amplitude Operators

From the equation of motion (Equation (7)) derived in the previous section, the motion amplitude $\hat{s}$ of the structure is found as shown in Equation (8). By relating this response amplitude to the amplitude of the incoming wave, the transfer function is defined in Equation (9):

$$\hat{s} = \frac{F_e}{-\omega^2(\mathrm{M} + \mathrm{A}) + \mathrm{i}\omega\mathrm{B} + \mathrm{C}} \tag{8}$$

$$\hat{Y} = \frac{\hat{s}}{\zeta_a} = \frac{F_e \,/\, \zeta_a}{-\omega^2(M + A) + i\omega B + C} \tag{9}$$

where ζ_a is the amplitude of the incident wave. The transfer function is also known as the response amplitude operator. It represents the response of the vessel to a unit wave. Accordingly, the unit of the RAO is m/m for the translational degrees of freedom and deg/m for the rotational ones.

As RAOs are related to a specific point of interest (POI), rigid body transformations are necessary to express the RAO for a changed location. In Equation (10) to (12), the transformation for the surge, sway and heave motion are shown. The rotational degrees of freedom are not affected by a change of the reference point.

$$x_{POI} = s_1 + \theta\Delta z - \psi\Delta y \tag{10}$$

$$y_{POI} = s_2 - \phi\Delta z + \psi\Delta x \tag{11}$$

$$z_{POI} = s_3 - \phi\Delta y + \theta\Delta x \tag{12}$$

where x_{POI}, y_{POI} and z_{POI} are the motions in the respective direction in the new point of interest. Δx, Δy and Δz are the distances between original reference point and the POI. ϕ, θ and ψ represent the rotational motions roll, pitch and yaw (Journée & Massie, 2001).

2.3 Radiation-Diffraction Analysis

To solve the equation of motion and, therefore, define the RAOs, the missing variables such as the added mass matrix *A*, the damping terms *B* and the excitation force need to be determined by finding all forces acting on the body. For this, marine structures are categorized into two groups depending on their relative size to the waves they encounter: Small and slender structures are considered not to influence the incoming waves, whereas large structures lead to a disturbance. To determine the category of a structure, a threshold of $0.2\,\lambda$ is defined where λ is the wavelength. For small structures with a dimension of the main cross section of $D < 0.2\,\lambda$, the drag and inertia forces have a large influence. If the reference dimension is larger than the threshold, the diffraction forces are the main force components and viscous effects are negligible in first instance (see section 2.4 for further details on viscous effects).

The forces acting on a body can be calculated in a radiation-diffraction analysis. The potential flow theory is applied where the fluid is assumed to be incompressible, irrotational and inviscid. The diffraction problem, which considers the forces due to the incoming wave assuming that the vessel is fixed, and the radiation problem, which describes the forces due to a forced oscillation of the vessel without any incident waves, can be treated separately. As shown in Figure 5: Radiation-Diffraction Problem , the resulting motions can be found by superimposing the wave loads and the hydromechanical loads.

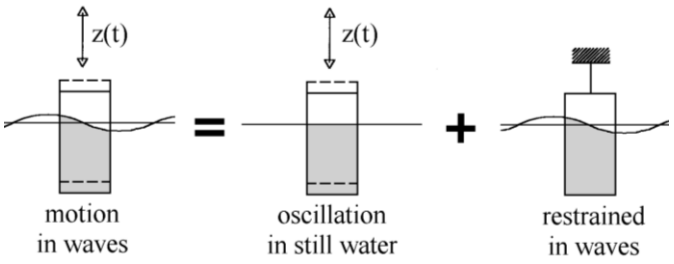

Figure 5: Radiation-Diffraction Problem (Journée & Massie, 2001)

In the diffraction problem, the wave excitation forces are determined. As mentioned in the previous section, this includes the Froude-Krylov and the diffraction force. The Froude-Krylov force is determined by integrating the pressure field of the wave over the body. For this, the wave is considered to be undisturbed. To account for the effect of the structure on the wave, the diffraction force is calculated. By solving the radiation problem, the hydromechanical loads like the added mass, the damping and the restoring forces are calculated. For this, the ship is represented by a mass-spring-damper system with a forced oscillation (Journée & Massie, 2001).

To find the described forces acting on the surface of the vessel, the hull is divided into small elements by defining a mesh over the surface. The forces are then determined individually by solving the equation of motion for each element and the total force acting on the ship is found by adding all partial forces.

2.4 Roll Damping

Generally, damping due to viscous effects can be neglected for large vessels as the contribution to the overall damping is very small. This holds true for all three translational degrees of freedom, as well as for yaw and pitch. In contrast, viscous damping has a significant influence on the roll motion and, therefore, cannot be neglected.

Devolder et al. (2020) assessed the roll damping behavior of the *Orion* and determined coefficients to account for viscous roll damping. This was done using the Computational Fluid Dynamics (CFD) software OpenFOAM and the Harmonic Excited Roll Motion (HERM) technique which is a method to estimate roll damping coefficients for large roll motions. For this, an external moment is applied to the ship in the simulations representing a rotating mass that leads to roll motions.

2.5 Wave Energy Spectra

Irregular sea states can be modelled by superimposing sinusoidal waves of different wave heights and periods. Reversed, these sinusoidal wave components can be found from an irregular sea using Fourier transformation. Wave energy spectra are used to represent these random seas by defining the energy distribution of the sea state across the underlying wave frequencies. Multiple mathematical definitions of energy spectra applicable to different wave climate characteristics are available. The most popular spectra are the Pierson-Moskowitz and the JONSWAP spectrum (Molland, 2008).

These standard energy spectra $S(\omega_n)$ are defined by the wave amplitude ζ_n as shown in Equation (13). The area of one increment $\Delta\omega$, which represents regular waves within the frequency range $\Delta\omega$, is equal to half of the squared wave height ζ_n of the wave of frequency ω_n.

$$S(\omega_n) \cdot \Delta\omega = \frac{1}{2}\zeta_n^2 \tag{13}$$

The JONSWAP spectrum is used in this thesis to represent the sea state defined by the significant wave height H_s and the zero-crossing period T_z found in the scatter diagrams. This spectrum was developed during the Joint North Sea Wave Program and, as the name suggests, it is based on wave data measured in the North Sea (Hasselmann, Barnett, Bouws, Calson, & Cartwright, 1973). The JONSWAP spectrum $S_J(\omega)$ is derived from the Pierson-Moskowitz spectrum $S_{PM}(\omega)$ as shown in Equations (14) to (16):

$$S_J(\omega) = A\, S_{PM}(\omega)\, \gamma^{\left(exp\left(-0.5\left(\frac{\omega-\omega_p}{\sigma\omega_p}\right)^2\right)\right)} \tag{14}$$

$$S_{PM}(\omega) = \frac{5}{16} \cdot H_S^2 \cdot \omega_p^4 \cdot \omega^{-5} exp\left[-\frac{5}{4} \cdot \left(\frac{\omega}{\omega_p}\right)^{-4}\right] \tag{15}$$

$$A = \frac{0.2}{0.065\,\gamma^{0.803} + 0.135} \tag{16}$$

where A is a normalization factor, H_s is the significant wave height, $\omega_p = 2\pi/T_p$ is the angular spectral peak frequency and σ is the spectral width parameter. For these parameters, average values found during the data collection can be used: $\sigma_a = 0.07$ for $\omega \leq \omega_p$ and $\sigma_b = 0.09$ for

$\omega > \omega_p$ (DNVGL-RP-C205) . The peak shape parameter γ is introduced to account for the fact that sea states are generally not fully developed as assumed in the Pierson-Moskowitz spectrum. A standard value of $\gamma = 3.3$ is usually considered.

The significant wave height H_s is defined as the mean value of the highest third of all wave heights and the peak period T_p as the inverse of the peak frequency of the wave energy spectrum meaning it is the period associated with the most energetic wave in the sea state (Hapel, 1990).

To determine characteristic variables of an energy spectrum $S(\omega)$, the spectral moments are calculated. They are defined as shown in Equation (17), where m_j is the *j*th moment of the energy spectrum. From the zeroth and second spectral moment, the mean zero-upcrossing period T_z can be determined as shown in Equation (18). The significant wave height, defined by double the significant amplitude, is related to the zeroth spectral moment m_0 as given in Equation (19) (Clauss, 2002).

$$m_j = \int_0^\infty S(\omega)\omega^j d\omega \tag{17}$$

$$T_Z = 2\pi \sqrt{\frac{m_0}{m_2}} \tag{18}$$

$$H_S = 4\sqrt{m_0} \tag{19}$$

Wave energy spectra can be defined in dependency of the wave frequency only, as described previously in this section, or in three dimensions by adding the dependency of wave directions. This distinction is necessary due to the different types of waves found in the sea: swell waves, which are waves that travelled a long distance and were caused by storms in far away areas, and wind waves, which are generated by local winds. Generally, swell waves are long-crested waves

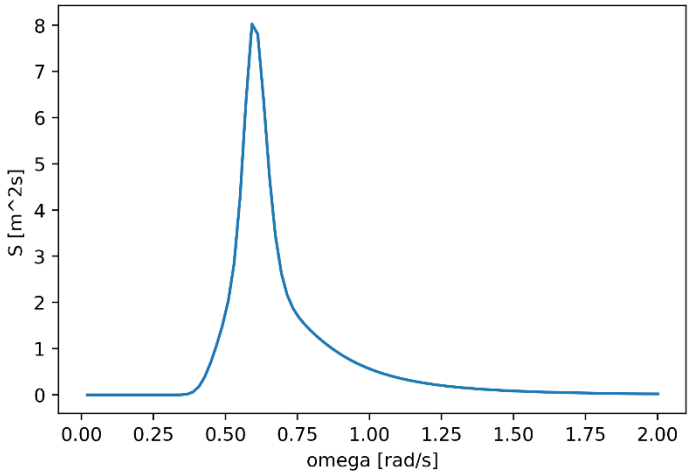

Figure 6: 2D JONSWAP Spectrum

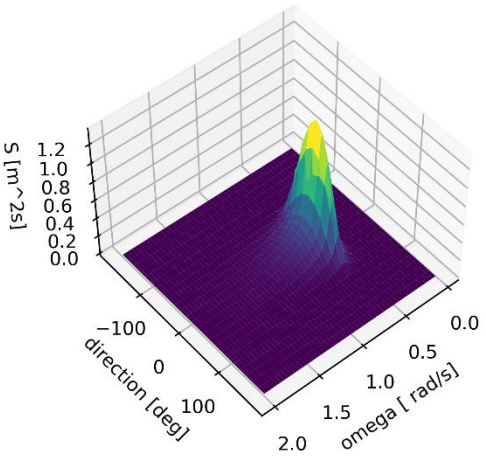

Figure 7: 3D JONSWAP Spectrum

The peak period T_p, used to define the JONSWAP spectrum can be determined from the zero-upcrossing period T_z and the peak shape parameter γ as shown in Equation (20) (DNVGL-RP-C205).

$$T_P = \frac{T_z}{0.6673 + 0.05037\gamma - 0.00623\gamma^2 + 0.0003341\,\gamma^3} \tag{20}$$

2.6 Response Spectra

A response spectrum relates the response amplitude operator and the wave energy spectrum as shown in Equation (21):

$$S(\omega) = \left|\frac{\hat{s}}{\zeta_a}(\omega)\right|^2 \cdot S_\zeta(\omega) \tag{21}$$

where ω is the wave frequency, $S_\zeta(\omega)$ is the wave energy spectrum and $\left|\frac{\hat{s}}{\zeta_a}(\omega)\right|$ is the RAO. Therefore, it shows the response of a vessel within a pre-defined sea state (Journée & Massie, 2001). The response spectrum can be determined for the motion, velocity and acceleration in all 6 degrees of freedom.

2.6.1 Acceleration Response Spectra

The acceleration response spectra are determined from the acceleration RAOs of each degree of freedom and the defined sea state. For this, the RAOs are squared and multiplied with the wave energy spectrum $S_\zeta(\omega)$ (see Equation (21)). As the JONSWAP spectrum can be defined in two dimensions or three dimensions, also the response spectrum can be expressed in 2D or 3D depending on the considered wave spectrum. Examples of both are shown in Figure 8 and Figure 9 representing the response to a sea state of H_S = 0.5 m, T_p = 3.5 s with a spreading of $n = 5$ for the 3D case for loading condition 1 and a wave encountering angle of 105 degrees.

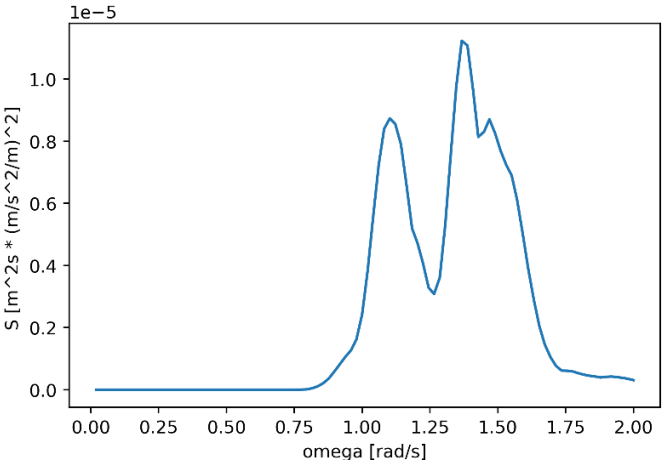

Figure 8: 2D Acceleration Response Spectrum (Surge)

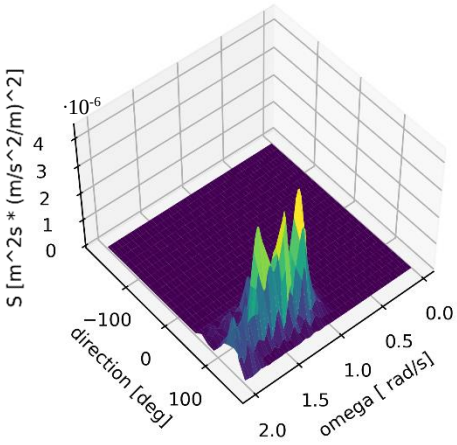

Figure 9: 3D Acceleration Response Spectrum (Surge)

2.6.2 Significant Accelerations

From the acceleration response spectrum, the significant accelerations a_S in a sea state are calculated for every degree of freedom as shown in Equation (22). For this, the zeroth spectral moment $m_{0,a}$ needs to be known. It can be calculated as previously shown for the wave spectrum in Equation (17).

$$a_S = 2\sqrt{m_{0,a}} \tag{22}$$

3 FATIGUE

In this chapter, the general concepts of fatigue are explained. A definition of fatigue is given first, introducing the causes of fatigue, the phases of fatigue failure and approaches to determine a component's fatigue life. Common hot spot locations and ways of improving the fatigue capacity are discussed. Next, the Characteristic S-N Curve approach is described in more detail by presenting S-N curves and Miner's rule. Three methods to determine the reference stress range used in the fatigue calculations are shown. Namely, the considered reference stress could be the nominal stress, the hot spot stress or the notch stress. The rainflow counting method is introduced as an example of cycle counting techniques and the Monte Carlo method is presented as a way to simulate the fatigue life of a structural component.

3.1 Definition of Fatigue

Cyclic loading of a structural member leads to repeated stressing of the structure's material. The stressing then leads to cracks in the material, growing of those cracks and finally to failure. This cumulative damage of a structure is called fatigue. Fatigue is a common failure mechanism for marine structures just like for any engineering structure (Tupper, 2013).

Causes for cyclic loads in ships and offshore structures are waves, wind, vortex-induced-vibrations, and other environmental impacts. As fatigue damage occurs in stress ranges that are lower than the yield strength of a material, even small loads can contribute to the fatigue (Bai, 2003). Fatigue failure is generally divided into two categories: high cycle fatigue and low cycle fatigue. If a structure fails with less than 10^4 loading cycles, it is referred to as low cycle fatigue. It is caused by high stresses that can be in the plastic range. Failures with more than 10^4 loading cycles are categorized as high cycle fatigue. In this case, the stress ranges are significantly lower than for the cases of a short fatigue life and mainly in the elastic regime (Paik, 2018).

The fatigue life of a structure is defined by three stages of fatigue: the crack initiation, the crack growth, and the fatigue fracture. In the first stage, crack development is initiated by plastic deformations of the material. Cracks generally start developing in areas of stress concentrations, for example at defects of the material. Next, the crack starts propagating. At first, this happens at a microstructural level where cracks are shorter than the grain size of the material. In this

stage, the crack propagation is highly influenced by grain boundaries which may lead to a temporary stop of crack growth. Nevertheless, the crack will keep propagating when the stress induced by the cyclic loading increases high enough. When a critical crack size is reached, the component fails due to fracture (Zerbst, Madia, Vormwald, & Beier, 2018). As this happens suddenly and often without major signs of damage before fracture, fatigue failure can be catastrophic (Chandrasekaran, 2018).

To assess a component's fatigue life, the Fracture Mechanics Approach or the Characteristic S-N Curve Approach can be used. In the Fracture Mechanics Approach, the fatigue life is estimated by assessing the crack propagation stage. For this, an initial crack is assumed to be developed already and the cycles until a certain defect size limit is reached are determined. For the Characteristic S-N Curve Approach, the fatigue damage is calculated based on S-N curves and Miner's rule as shown in Ch. 3.3 and 3.4 (Rigo & Rizzuto, 2003).

3.2 Critical Fatigue Locations

Fatigue analyses are essential for every location where fatigue damage is predicted to ensure the integrity of the overall structure. To predict these critical areas, general locations of fatigue should be checked. An example of these typical hot spots are areas of stress concentrations such as ones caused by welds. Important factors influencing the fatigue damage are residual stresses in the analyzed structure and the presence of defects. Also, the material properties and the dimensions of the structural detail play a role for the fatigue life (Fricke, 2017).

During the design and manufacturing, the expected fatigue damage can be reduced by following the following recommendations: The design of any structural component should avoid stress concentrations as much as possible. This can be achieved by optimizing the shape of cut-outs, increasing the wall-thickness in areas of high loads or adjusting brackets to allow a better transfer of forces between components. Geometric discontinuity or misalignment should be avoided.

During fabrication, stress concentrations can be avoided mainly by focussing on welded joints and reducing the residual stress. Ways to improve fatigue capacity of the weld include adjusting the weld geometry and removing defects within the weld. This can be achieved by grinding of

the weld to create a continuous transition between the two connected parts. An alternative to this is erosion with high-pressure water jets to modify the weld geometry (Bai, 2003).

3.3 S-N Curves

An S-N curve is a graph showing the stress range of a loading cycle with the corresponding number of repetitions until fatigue failure. Mean S-N curves are obtained by experiments. To define the ones used for design, the curves are lowered by two standard deviations to reach a survival probability of 97.7%. S-N curves can be defined as shown in Equation (23):

$$log\ N\ =\ log\ \bar{a}\ -\ m\ log\ \Delta\sigma \tag{23}$$

where N is the number of loading cycles to failure, log $\bar{a}$ is the intercept of the curve with the N-axis, m is the slope of the S-N curve and $\Delta\sigma$ [MPa] is the stress range. The stress range $\Delta\sigma$ is commonly denoted by S, explaining the name of the curve. The S-N curves provided by DNV (see Figure 10) are bi-linear which leads to a change of slope at 10^7 cycles and consider only the high cycle fatigue range.

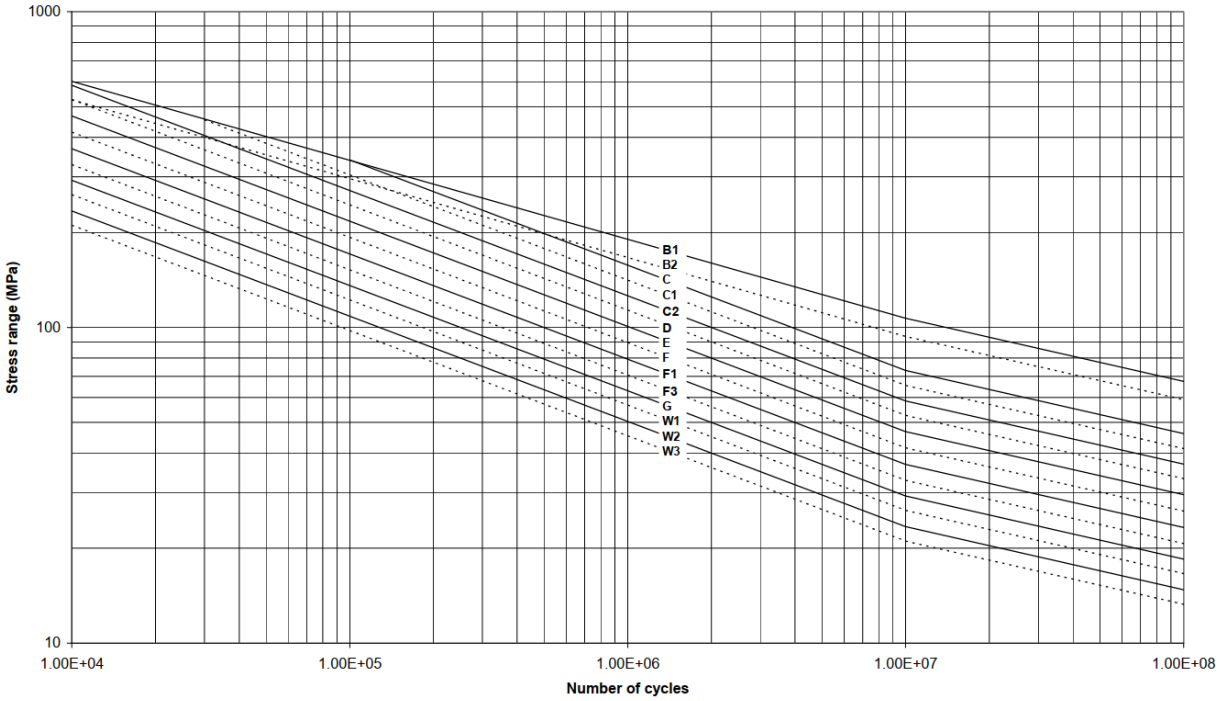

Figure 10: S-N curves in Air (DNVGL-RP-C203)

The fatigue life of a structure is not only dependent on the stress range and number of loading cycles but also on the specific structural detail and on the environmental conditions. Therefore, in the DNV rules, different graphs are defined for components in air and in seawater. As shown in the example in Figure 10, 14 S-N curves are given in each of the graphs to account for the different geometries as well as for different manufacturing and calculation methods (DNVGL-RP-C203).

Some materials, such as steel, have a fatigue limit (also known as endurance limit). This means that cyclic loads lower than the specific limit stress do not contribute to the fatigue damage of the structure. Thus, failure will never occur if all stresses stay lower than the fatigue limit and the fatigue life is infinite (Paik, 2020). In the DNV rules (DNVGL-RP-C203), the fatigue limit is defined at 10^7 loading cycles even though the S-N curve is not parallel to the x-axis after this point. Still, no detailed fatigue analysis is required if all stress cycles are of lower value than the fatigue limit.

3.4 Miner's Rule

According to Miner (1945), fatigue damage is cumulative meaning that effects of variable amplitude loading can be determined by adding up the effects of constant amplitude stress blocks. This rule is based on the assumption that a structure fails when it has absorbed the maximum possible amount of work. In this process, work-hardening of the material is neglected, and failure is defined as the initiation of a crack. All loading cycles are considered to be sinusoidal.

Using S-N curves, the partial damage *d* of a constant amplitude stress block can be calculated as shown in Equation (24). from the maximum number of cycles *N* at the current stress range and the actual number of cycles *n*. The failure criterion is defined in Equation (25). Therefore, the structural component will fail due to fatigue if the sum of all partial damages *D* is larger or equal to 1.

$$\frac{n}{N} = d \tag{24}$$

$$\sum \frac{n_i}{N_i} = \mathrm{D} \geq 1 \tag{25}$$

To summarize, Miner's rule is an integral part of fatigue calculations using the S-N Curve Approach. First, the partial damage per stress block is determined. Next, the damage of all stress blocks is summed to determine the total damage. If this value exceeds 1, the formation of cracks and, therefore, failure of the structure is expected.

3.5 Stress Range Calculation

To estimate the fatigue damage based on the S-N curve approach and Miner's assumption of cumulative damage, the stress range that a structure is subjected to during each loading cycle needs to be determined. For this, several methods are available. The three most commonly used approaches, which are the nominal stress approach, the hot spot stress approach and the notch stress approach, are presented in this section. In Figure 11, the mentioned stresses are graphically defined.

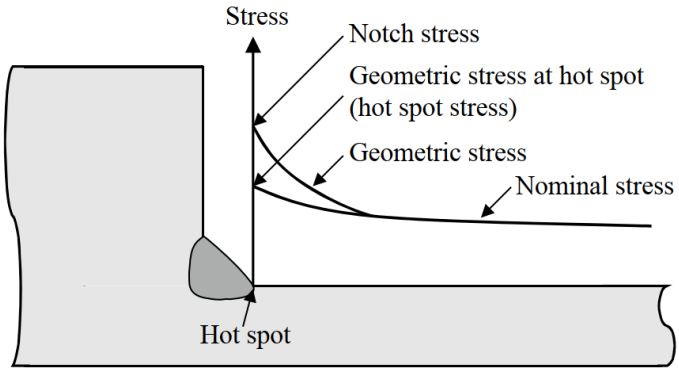

Figure 11: Stress Definition at Hot Spot (Paik, 2020)

3.5.1 Nominal Stress Approach

In the nominal stress approach, an average stress far away from the hot spot is considered as the reference stress (as shown in Figure 11). The stress concentration due to the specific structural configuration, like the geometry and welds, is neglected at first when determining the stress range (Paik, 2020). For this reason, the effects of the structural detail must be accounted for in the chosen S-N curve (Paik, 2018). In addition, a stress concentration factor *SCF* needs

to be applied to the nominal stress $\sigma_{nominal}$ to determine the local stress σ_{local} at a point of interest (Chandrasekaran, 2018). The calculation is shown in Equation (26 (DNVGL-RP-C203).

$$\sigma_{local} = SCF \cdot \sigma_{nominal} \tag{26}$$

To summarize, the general procedure of the nominal stress approach is described in the following (Liu, Yue, Geng, Wen, & Yan, 2018):

1. Identification of critical fatigue locations
2. Calculation of nominal stress and the stress concentration factor for each location
3. Selection of S-N curve according to the specific structural detail
4. Calculation of the fatigue damage from the local stress and the selected S-N curve using Miner's rule

An advantage of the nominal stress approach is that the nominal stress can be calculated by simple means such as beam theory. Finite element analyses are optional. This reduces the amount of work significantly (DNVGL-RP-C203). The main disadvantage is the need to determine the stress concentration factor which requires detailed information about the structural detail. Values for this can also be found in rules of classification societies (Liu, Yue, Geng, Wen, & Yan, 2018).

3.5.2 Hot Spot Stress Approach

The hot spot stress used in the hot spot stress approach is defined as the stress in a location where crack initiation is expected. It includes geometrical effects but not those of a potentially present weld. Stress concentrations induced by welds need to be considered by selection of an S-N curve suitable for the current structural detail (Paik, 2018).

There are two options to determine the hot spot stress: In the first one, a stress concentration factor is used to obtain the hot spot stress value from the nominal stress. The second option is using a finite element analysis to determine the stress at the hot spot. For this, the mesh needs to be fine enough to compute the hot spot stress accurately (Roh & Lee, 2018).

The main advantage of the hot spot stress approach is that the reference stress used for the fatigue calculations can be determined directly with a finite element analysis. In this case, no stress concentration factor needs to be determined. Still, this method can lead to a greater

workload than the nominal stress method as the preparation of the finite element model takes time (Niemi, Fricke, & Maddox, 2018). Nevertheless, if a finite element model is available, it can be useful to determine the hot spot locations (Garbatov, Rudan, Gaspar, & Guedes Soares, 2011).

3.5.3 Notch Stress Approach

The stress value used in the notch stress approach includes effects both of the geometry and the weld. It is therefore the total stress present at a weld toe. The notch stress can be determined by using FEM and applying a notch stress factor to the results of the finite element analysis (Paik, 2020). To determine the notch stress, following limitations should be followed: The approach should be used only for fatigue calculations of welds with expected cracks starting at the toe or root of the weld. Also, the minimum plate thickness is limited to 5 mm (Bai, 2003).

An advantage of fatigue calculations using the notch stress is the very specific result: The input data to calculate the notch stress is chosen for one specific hot spot geometry and, therefore, a stress concentration factor is not needed. On the downside, the dimensions of the actual built structure need to be known exactly and, consequently, the manufacturing tolerances are low (Paik, 2018).

3.6 Stress Cycle Counting

As for the calculation of the stress range, there are several available methods to determine the number of stress cycles. Monte Carlo simulations are introduced to obtain stress cycles from variable loadings defined by probability distributions. The rainflow counting method can determine stress cycles from a given stress history. Simplified methods, such as the Lambda Factor method, provide equivalent stress cycles to be used in cases where a loading history is not available.

3.6.1 Monte Carlo Simulations

The Monte Carlo method developed by Metropolis and Ulam (1949) is a statistical approach to numerically find solutions to problems that are hardly or not solvable using analytics. This is

done by making use of the law of large numbers and repeating a calculation with probabilistically defined input a large number of times. By randomly sampling the input variables of the defined problem from a collection following the specified probabilities, a probability distribution of solutions is found. The Monte Carlo method therefore allows for numerical solutions of problems using a mixed stochastic and deterministic approach.

For fatigue analyses, Monte Carlo simulations are a common tool used to determine the number of stress cycles expected due to statistically defined loading conditions. For ships and offshore structures, the spectral fatigue analysis can be applied to study the effect of waves, which are the main variable loads on most structures in the sea, on the fatigue life. The sea spectra are combined with the response amplitude operators of the structure to find its dynamic behavior in the sea and determine the experienced stress cycles for the fatigue calculations. In the short-term, the sea is considered to be stationary. The long-term variation of the waves is provided by scatter diagrams which define the relative probabilities of different sea states and, therefore, give one of the collections sampled from during the Monte Carlo simulation (Yeter, Garbatov, & Guedes Soares, 2014).

3.6.2 Rainflow Counting Method

Matsuishi and Endo (1968) developed the rainflow counting method to extract blocks of constant amplitude stresses from a random load history. This is done to define stress ranges and occurrences that can be used in fatigue estimations. The presented algorithm sorts the random stress events into blocks of constant stress ranges by identifying closed stress-strain hysteresis loops in the loading history. These hysteresis loops are typical for the stress-strain response of metals when loaded and unloaded. The rainflow method is analogous to rain running down the levels of a pagoda roof. For this, the stress history graph is turned by 90 degrees as shown in Figure 12.

The stress cycles are identified by following the path that rain would run down a roof: The starting point is the largest peak or valley of the stress history. The path is followed down the roof until the rain does not fall on a lower level anymore (see point D in Figure 12). From this point, the procedure is repeated in the opposite direction until the rain off the roof completely. Then, a new starting point that is now the largest peak or valley and has a path that has not been followed yet is chosen. The rain falls until there is no next level anymore or until is reaches a level previously encountered in another cycle. This procedure is then reversed again. Each of

these stress reversals represent a full loading cycle. All steps are repeated until the rain has reached all parts of the roof meaning that all loading cycles have been considered. This way, the stress ranges and their number of repetitions for a time-domain fatigue analysis are determined (Wallbrink & Hu, 2010).

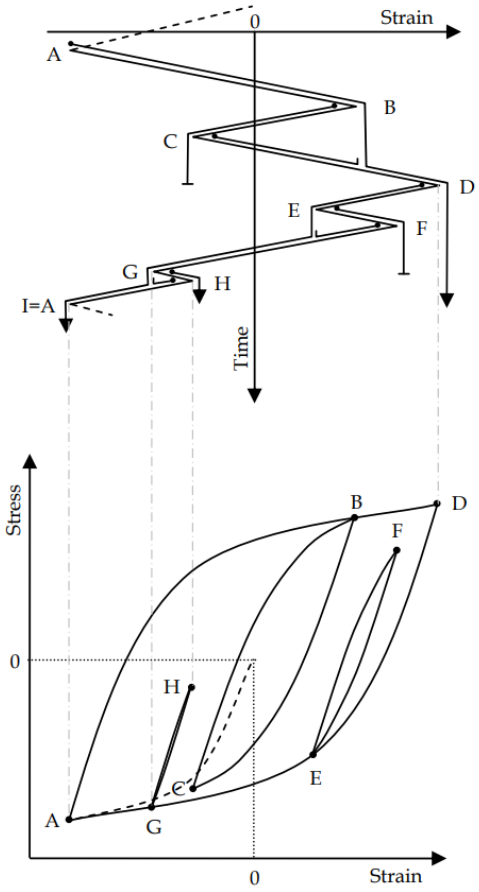

Figure 12: Rainflow Counting and Stress-Strain Hysteresis (Wallbrink & Hu, 2010)

4 METHODOLOGY

The aim of this thesis is to analyze the fatigue of the monopile seafastening of the *Orion* and investigate which methods are adequate for the analysis. For this, simplified fatigue estimation methods are developed to obtain a first estimation. Monte Carlo Simulations are applied, and the results are compared to the simplified approaches.

Before starting the fatigue calculations, the critical fatigue locations need to be known. In previous studies of DEME, hot spots for fatigue damage in the seafastening structure were determined. This was done by using finite element method and identifying areas of high stress concentrations or fluctuations.

Other necessary inputs for the calculations are the response amplitude operators of the vessel. ANSYS Aqwa is used to calculate the RAOs in 6 degrees of freedom in the center of gravity of the ship. The RAOs are then shifted to the center of gravity of the monopile located in the seafastening. The monopile's COG it is used as the reference point of the RAOs. For the Monte Carlo simulation, viscous roll damping coefficients are determined and added by post-processing the RAOs as these effects are not considered by ANSYS Aqwa.

Additionally, there are inputs to the fatigue calculations defining the environmental conditions. The possible sea states are represented by JONSWAP spectra with significant wave heights based on statistical data of different nautic zones defined by DNV. This data is given as scatter diagrams showing the relative probability of different combinations of significant wave heights H_S and peak periods T_P for a specific nautic zone. Also, possible wave encountering angles with relative probabilities are defined.

Multiple options of simplified fatigue analysis are explored to estimate the criticality of the fatigue damage of the structure. To take into account more detailed information on the actual operational profile, a simplified fatigue estimation method based on weighted sums is introduced. The goal of this method is to find the average fatigue damage of one hour that the vessel spends in every loading condition and in each nautic zone to then calculate the total damage by applying the results to the operational profile. The general procedure is described in the following:

1. Calculation of the partial fatigue damage for every possible H_S/T_P combination (within the defined limits of operation) given in the scatter diagram of each nautic area and for each loading condition
2. Calculation of expected damage for one hour spent in each analyzed zone/loading condition combination by finding the weighted average of the partial fatigue values according to their relative probability defined in the scatter diagram
3. Calculation of total fatigue damage by multiplying the partial damages by the number of hours spend in each nautic zone and loading condition as defined in the operational profile

Instead of using weighted sums to determine the fatigue damage per hour, Monte Carlo simulations are applied to go through the previously described steps of the fatigue estimation. The average fatigue damage in every zone is determined by simulating enough hours in each condition to reach convergence. The general procedure of this simulation is the same as for the full Monte Carlo method described in the following paragraphs except that in this method the calculations are repeated over the hours of one condition and not over the entire operational profile. The total fatigue damage is found by combining the partial damages with the operational profile as described for the weighted sum method.

To get more sophisticated results, Monte Carlo simulations are implemented in Python. The operational period is simulated repeatedly for as many times as it is necessary to find a converging solution. The underlying principle of this is the law of large numbers, making it possible to find the average expected fatigue damage. In each run of the simulation, motion analyses in the frequency domain are done for every hour of the operational lifetime that is spent at sea. For this, the operational information specifying the loading condition and nautic zone of the current hour are read in first. For each hour, the aforementioned inputs are pseudo-randomly selected based on their specified relative probability. A wave encountering angle is chosen to read in the corresponding RAO and shift it to the center of gravity of the monopile. Next, an H_S/T_P combination is selected based on the scatter diagram of the current nautic zone and a wave spectrum is generated. From the acceleration RAOs and the wave spectrum, a response spectrum is found which allows the computation of significant accelerations.

The Monte Carlo simulation outputs the significant accelerations of every degree of freedom and the significant stresses for every simulated hour. Also, the number of acceleration and stress cycles is given. From this output, histograms of the accelerations and stresses are calculated.

As an example, this process is described for the stress histogram: Based on all stresses found in the simulations, a specified number of stress bins is defined between the lowest and highest stress values. All stress occurrences are then sorted into the bins to find a histogram representing all simulations.

Using the average stress histogram, the fatigue damage can be calculated based on the S-N curve approach. The S-N curve is chosen from the DNV standard where curves for different applications are provided. For every bin, the maximum allowable number of stress cycles is determined based on the upper edge value of the stress bin. The partial fatigue damage of one bin is found from the maximum number of cycles at the defined stress range and the actual number of cycles. To obtain the total fatigue damage of the given operational profile, the partial damages are summed up according to Miner's rule.

5 CRITICAL FATIGUE LOCATIONS

5.1 Determined Hot Spots

6 OPERATIONAL CONSIDERATIONS

In this chapter the operational parameters of the study case are introduced. First, the considered loading conditions and the corresponding operational limits are defined. Next, the environmental conditions are discussed. For this, different nautic zones with associated scatter diagrams are presented and possible wave encountering angles of the ship are defined based on operational conditions. Lastly, the planned route is presented by defining loading.

6.1 Loading Conditions

6.2 Environmental Conditions

6.2.1 Nautic Zones

In the DNV rules, the worldwide seas are divided into 104 nautic zones as shown in Figure 13. For each of these zones, site-specific scatter diagrams are provided to define the wave climate in the different areas. In this thesis, the route of the ship will be defined by the hours spent in each of the nautic zones.

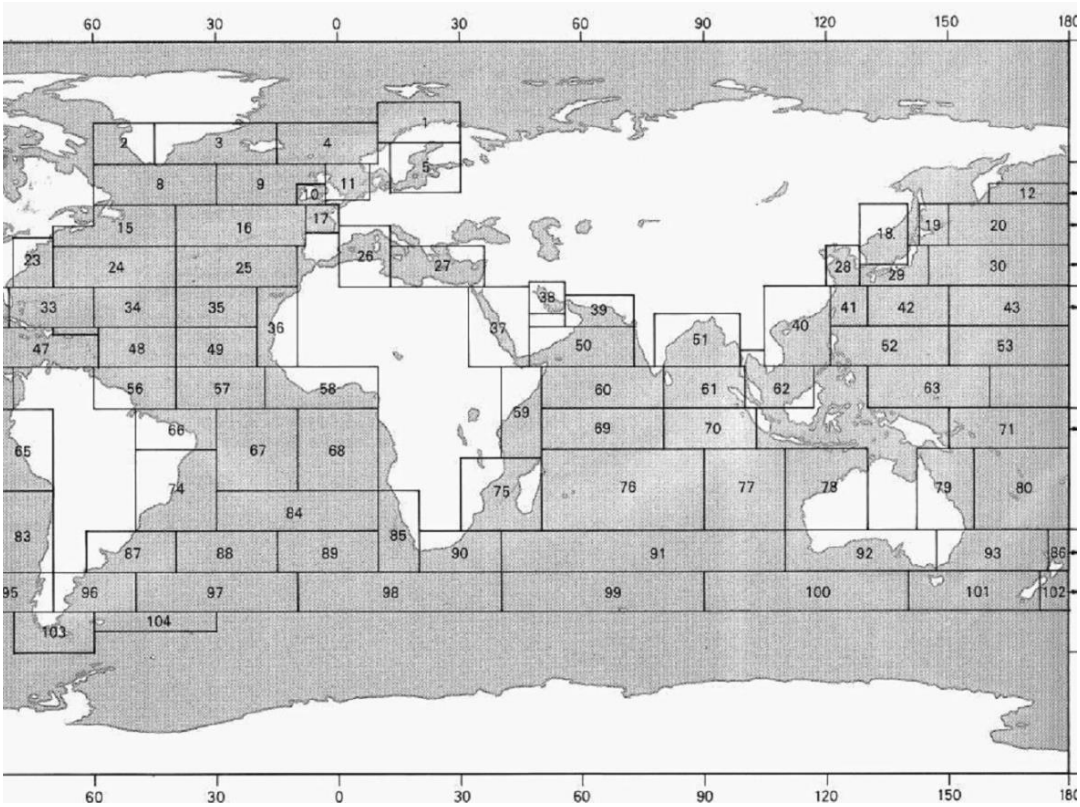

Figure 13: Nautic Zones (DNVGL-RP-C205)

6.2.2 Scatter Diagrams

Scatter diagrams are used to characterize a specific site's, or in this case nautic zone's, long-term wave climate. They provide the relative probabilities of H_s/T_z combinations for the nautical zones based on measured data that is sorted into H_s/T_z bins. Those bins are divided to significant wave heights H_s between 0.5 m and 10.5 m with steps of 1 m and zero-crossing periods T_z between 3.5 s and 13.5 s with steps of 1 s. As an example, the scatter diagram for the nautic area 11 defined by DNV is given in Table 1 (DNVGL-RP-C205). The main disadvantage of scatter diagrams is that they do not include seasonal or directional information. Instead, values are averaged over the year and all wave directions. Also, the size of the bins with H_s/T_z combinations can significantly influence calculations using scatter diagrams. This holds true especially for small significant wave heights (Folley, 2017).

Table 1: Scatter Diagram of Nautical Zone 11 (North Sea)

T_z [s] / H_s [m]	**3.5**	**4.5**	**5.5**	**6.5**	**7.5**	**8.5**	**9.5**	**10.5**	**11.5**	**12.5**	**13.5**
0.5	100	109	63	21	5	1	0	0	0	0	0
1.5	17	71	95	62	26	8	2	1	0	0	0
2.5	2	22	52	54	34	15	5	2	0	0	0
3.5	0	6	21	32	26	15	6	2	1	0	0
4.5	0	1	7	15	16	11	6	2	1	0	0
5.5	0	0	2	6	8	7	4	2	1	0	0
6.5	0	0	1	2	4	4	3	1	1	0	0
7.5	0	0	0	1	2	2	1	1	0	0	0
8.5	0	0	0	0	1	1	1	1	0	0	0
9.5	0	0	0	0	0	0	0	0	0	0	0
10.5	0	0	0	0	0	0	0	0	0	0	0
11.5	0	0	0	0	0	0	0	0	0	0	0
12.5	0	0	0	0	0	0	0	0	0	0	0
13.5	0	0	0	0	0	0	0	0	0	0	0
14.5	0	0	0	0	0	0	0	0	0	0	0

6.2.3 Wave Encountering Angles

6.3 Operational Profile

7 RADIATION-DIFFRACTION ANALYSIS

In a radiation-diffraction analysis using ANSYS Aqwa 2019 R3, the response amplitude operators of the *Orion* are determined. The setup with the chosen input parameters is given in the following and the resulting RAOs of the different loading conditions are presented.

7.1 Setup of ANSYS Aqwa

In the first step, the geometry of the hull needs to be defined. An existing model of the *Orion* is imported to ANSYS Workbench and a mesh is generated adopting mesh parameters of previous radiation-diffraction analyses done by DEME. From this, an initial .dat input file for Aqwa is created.

7.2 Response Amplitude Operators of the *Orion*

8 SIMPLIFIED FATIGUE ESTIMATION

For a first evaluation of the fatigue endurance of the monopile seafastening and to study the influence of different operational configurations, simplified fatigue estimation methods are applied. To take into account the operational profile and the statistical distribution of wave encountering angles, a weighted sum method is developed to determine the expected fatigue damage in the different nautic zones. As a transition to the full Monte Carlos simulation of the entire operational life, a simplified Monte Carlo approach is presented which is based on the previously developed weighted sum method.

8.1 Modified Method

8.2 Weighted Sum Method

8.2.1 Methodology

8.2.2 Implementation

8.2.3 Results

8.3 Simplified Monte Carlo Simulation

8.3.1 Methodology

8.3.2 Convergence Study

8.3.3 Results

9 FATIGUE ANALYSIS USING MONTE CARLO SIMULATIONS

9.1 Monte Carlo Simulation of Stresses

9.2 Calculation of Fatigue Damage

9.2.1 Selection of SN-Curve

9.2.2 Fatigue Damage per Stress Bin

9.2.3 Total Fatigue Damage

9.3 Class Diagram

9.4 Convergence Study

10 RESULTS OF FATIGUE ANALYSES

10.1 Benchmark Case

10.2 Effect of Viscous Roll Damping

10.3 3D JONSWAP Spectrum

10.4 Comparison of Possible Routes and Operational Profiles

10.5 Effect of Wave Encountering Angle

11 DISCUSSION OF RESULTS

11.1 Benchmark Case

11.2 Evaluation of Simplified Methods

11.3 Sensitivities of Fatigue Calculations

11.4 Limitations

12 CONCLUSIONS

12.1 Recommendations

12.2 Future Works

ACKNOWLEDGEMENTS

I am extremely thankful to my supervisors Benjamin and Florian who guided and supported me all throughout my internship at DEME. My appreciation extents to Dieter and Andrei who helped me with suggestions and insightful information for my thesis. Furthermore, I would like to thank all members of the naval team, namely Christophe, David, Elstine, Lachlan, Sijun and Thomas, for their valuable advice and encouragement.

I wish to thank the EMShip+ program with all associated professors and lecturers for giving me the opportunity to grow my knowledge and paving the way for my future career. Especially, I would like to thank Simone Saettone for his ongoing support during my time at UPM and his advice regarding my thesis. I would like to express my sincere gratitude to the Erasmus+ Program of the European Union for providing the funding of my Master's studies.

Last but not least, I would like to thank my family and friends for their support and belief in me all throughout my studies.

REFERENCES

Bai, Y. (2003). *Marine Structural Design.* Oxford: Elsevier Science Ltd.

Chandrasekaran, S. (2018). *Dynamic Analysis and Design of Offshore Stuctures* (2nd ed.). Singapore: Springer Nature.

Clauss, G. (2002). *Stochastische Analyse meerestechnischer Systeme.* Berlin: Technische Universitat Berlin.

DEME. (n.d.). *Orion - FACTS*. Retrieved 07 14, 2022, from https://www.deme-group.com/technologies/orion

Devolder, B., Stempinski, F., Mol, A., & Rauwoens, P. (2020). Roll Damping Simulations of an Offshore Heavy Lift DP3 Installation Vessel Using the CFD Toolbox OpenFOAM. *OMAE*.

DNVGL-RP-C203. (2016). *Fatigue design of offshore steel structures.*

DNVGL-RP-C205. (2019). *Environmental conditions and environmental loads.*

DNV-ST-N001. (2021). *Marine operations and marine warranty.*

EN 1993-2. (2006). Eurocode 3: Design of Steel Structures, Part 2: Steel Bridges. European Committee for Standardization.

Faltinsen, O. M. (1998). *Sea Loads on Ships and Offshore Structures.* Cambridge: Cambridge University Press.

Folley, M. (2017). The Wave Energy Resource. In A. Pecher, & J. P. Kofoed (Eds.), *Handbook of Ocean Wave Energy* (pp. 43-80). Springer Nature.

Fricke, W. (2017). Fatigue and Fracture of Ship Structures. *Encyclopedia of Maritime and Offshore Engineering*.

Garbatov, Y., Rudan, S., Gaspar, B., & Guedes Soares, C. (2011). Fatigue Assessment of Marine Structures. *Marine Technology and Engineering*, 865-888.

Hapel, K.-H. (1990). *Festigkeitsanalyse dynamisch beanspruchter Offshore-Konstruktionen.* Braunschweig: Friedr. Vieweg & Sohn Verlagsesellschaft mbH.

Hasselmann, K., Barnett, T., Bouws, E., Calson, H., & Cartwright, D. (1973). *Measurements of wind-wave growth and swell decay during the Joint North Sea Wave Project (JONWAP).* Hamburg: Deutsches Hydrographisches Institut.

Journée, J. M., & Massie, W. W. (2001). *Offshore Hydromechanics.* Delft: Technical University of Delft.

Lewis, E. V. (Ed.). (1989). *Priciples of Naval Architecture - Volume III - Motions in Waves and Controllability* (2nd ed.). Jersey City: The Society of Naval Architects and Marine Engineers.

Liu, J., Yue, Z., Geng, X., Wen, S., & Yan, W. (2018). *Long-Life Design and Test Technology of Typical Aircraft Structures.* Singapore: Springer Nature.

Maddah, N., & Nussbaumer, A. (2012). Evaluation of Eurocode damage equivalent factor based on traffic simulation. *Proc. of the 6th Int. Conf. on Bridge Maintenance, Safety and Management.*

Matsuishi, M., & Endo, T. (1968). Fatigue of metals subjected to varying stress. *Japan Society of Mechanical Engineers, 68*(2), 37-40.

Metropolis, N., & Ulam, S. (1949). The Monte Carlo Method. *Journal of the American Statistical Association, 44*(247), 335-341.

Miner, M. A. (1945). Cumulative Damage in Fatigue. *Journal of Applied Mechanics*, 159-164.

Molland, A. F. (Ed.). (2008). *The Maritime Engineering Reference Book - A Guide to Ship Design, Construction and Operation.* Butterworth-Heinemann.

Newman, J. (1977). *Marine Hydrodynamics.* Cambridge, Massachusetts: The MIT Press.

Niemi, E., Fricke, W., & Maddox, S. J. (2018). *Structural Hot-Spot Stress Appraoch to Fatigue Analysis of Welded Components* (2nd ed.). Singapore: Springer Nature.

Paik, J. K. (2018). *Ultimate Limit State Analysis and Design of Plated Structures* (2nd ed.). Hoboken, NJ: John Wiley & Sons.

Paik, J. K. (2020). *Advanced Structural Safety Studies.* Singapore: Springer Nature.

Rigo, P., & Rizzuto, E. (2003). Analysis and Design of Ship Structure. In *Ship design and construction* (pp. 18-1).

Roh, M.-I., & Lee, K.-Y. (2018). *Computational Ship Design.* Singapore: Springer Nature.

Śledziewski, K. (2017). FATIGUE ASSESSMENT OF BRIDGE STRUCTURES ACCORDING TO EUROCODES. *JOURNAL OF CIVIL ENGINEERING, ENVIRONMENT AND ARCHITECTURE*, 187-206.

Tupper. (2013). *Introduction to Naval Architecture* (5th ed.). Oxford: Butterworth-Heinemann.

Wallbrink, C., & Hu, W. (2010). *A Strain-Life Module for CGAP: Theory, User Guide and Examples.* DSTO Defence Science and Technology Organisation .

Yeter, B., Garbatov, Y., & Guedes Soares, C. (2014). Spectral fatigue assessment of an offshore wind turbine structure. *Developments in Maritime Transportation and Exploitation of Sea Resources*, 425-433.

Zerbst, U., Madia, M., Vormwald, M., & Beier, H. (2018). Fatigue strength and fracture mechanics – A general perspective. *Engineering Fracture Mechanics*(198), 2-23.

APPENDIX

A1 Response Amplitude Operators

A2 Validation of Response Spectra

A3 Weighted Sum Method